A Highly Sensitive Narrowband Nanocomposite Photodetector with Gain

*Liang Shen, Yanjun Fang, Haotong Wei, Yongbo Yuan, and Jinsong Huang**

Highly sensitive photodetectors with narrowband response have wide applications in the fields of fluorescence microscopy, spectroscopy, clinical chemistry, imaging, chemical/environmental/elemental analysis, and the scientific research.[1–5] As an example of biologic application, the fluorescence study of the stained cells is generally used to visualize the targeted cells and to accurately determine the position and the concentration of stained cells. This needs photodetectors that can selectively sense the fluorescence emission generated by stained cells while reject background emission or excitation light. However, it is difficult to find a semiconductor material, including both traditional semiconductors or emerging organic semiconductors, with a very narrow absorption spectrum.[6,7] To solve this issue, a bandpass optical filter is generally used to select a wavelength band of interest to combine with a broadband photodetector. However, it is noted that the commercially available optical filters do not always cover the spectral band of interest for different applications. In addition to the cost added by the bandpass optical filters and increased sensor size and weight, there are issues with interference-based filters such as contamination and shoulder absorption.

Recently, a new type of narrowband photodetectors without bandpass optical filters has been reported using relatively thick organic bulk-heterojunction (BHJ) films.[5] The idea is to take advantage of the difference of light attenuation length at different wavelength to realize the wavelength-dependent charge collection, which is illustrated in **Figure 1**a. The absorption coefficient of any photoactive material is wavelength dependent. Generally, the absorption close to or below the optical bandgap is much weaker than the above-bandgap absorption, and thus longer wavelength light has a larger penetration depth (L_p) in the photoactive layer,[8] causing a variation of charge-generation region with respect to incident light wavelength, which is shown in Figure S1a,b (Supporting Information). Generally, charges generated by short- and long-wavelength light are efficiently collected by electrodes in thin-film (80–200 nm) polymer solar cells. However, when the photoactive layer is much thicker (2–5 μm), the photogenerated charges by shorter wavelength light might not be collected by the electrodes because of the too small charge-drift length (L_d). The photogenerated charges end up with charge recombination when the sum of L_p and the charge-drift length is less than the film thickness (L_f). On the other hand, the charges photogenerated by long-wavelength light, which have smaller absorption coefficient and thus a longer penetration depth, have a chance to be partially collected by the electrodes. As a result, the thick active layer devices have photoresponse only to long-wavelength light, but small or no response to short-wavelength light, resulting in a wavelength-dependent photoresponse (or external quantum efficiency, EQE) peak close to the band edge as illustrated in Figure 1a. This new mechanism allows us to achieve narrowband light detection by engineering L_p, L_d, and L_f.

We did a simulation to find out the charge-generation region using a classical polymer semiconductor material system of poly(3-hexylthiophene) (P3HT):[6]-phenyl C60 butyric acid methyl ester (PCBM) in a device with the structure of indium tin oxide (ITO)/poly(*N*-vinylcarbazole) (PVK) (20 nm)/P3HT:PCBM (3.5 μm)/2,9-dimethyl-4,7-diphenyl-1,10-phenanthroline (BCP) (10 nm)/aluminum (Al) (100 nm). Figure 1b shows the distribution of normalized modulus square of optical electric field ($|E(x)^2|$) in the active layer. The color difference represents the $|E(x)^2|$ intensity. The $|E(x)^2|$ is almost zero below 630 nm at a distance of 500 nm from ITO, suggesting that light below 630 nm is almost completely absorbed by the 500 nm P3HT:PCBM layer due to their much shorter L_p. On the other hand, strong oscillation of $|E(x)^2|$ around 680 and 720 nm appears across the whole film due to the interference effect and larger L_p.

One limitation of this device structure for narrowband photodetection is that the responsivity of the photodetectors is relatively low, because a significant amount of photogenerated charges close to the transparent electrode cannot be collected by the counter electrode. The reported maximum EQE was less than 35% at −1 V with the active layer thickness of 1500 nm based on the PCDTBT:$PC_{71}BM$ system in ref. [5]. We did computation of the EQE by assuming that all the charges generated within L_d from the Al cathode can be completely collected and derived the EQE spectrum of the thick P3HT:PCBM device. The detailed simulation process can be found in the Supporting Information. As shown in Figure 1c, the theoretical EQE upper limit is less than 20% for a −6 V biased device with the active layer thickness of 3 μm based on the P3HT:PCBM system. The small responsivity may limit the applications of these narrowband photodetectors. Here, we report a >20-folds improvement of the EQE to these narrowband photodetectors by introducing charge traps into the photoactive layer, which also resulted in a large linear dynamic range (LDR) of 110 dB and a low-noise equivalent power (NEP) of 5 pW cm^{-2}.

The device structure and working principle are shown in **Figure 2**. To achieve a large photoconductive gain in the

Dr. L. Shen, Dr. Y. Fang, Dr. H. Wei,
Dr. Y. Yuan, Prof. J. Huang
Department of Mechanical and Materials Engineering
Nebraska Center for Materials and Nanoscience
University of Nebraska–Lincoln
Lincoln, NE 68588-0656, USA
E-mail: jhuang2@unl.edu

DOI: 10.1002/adma.201503774

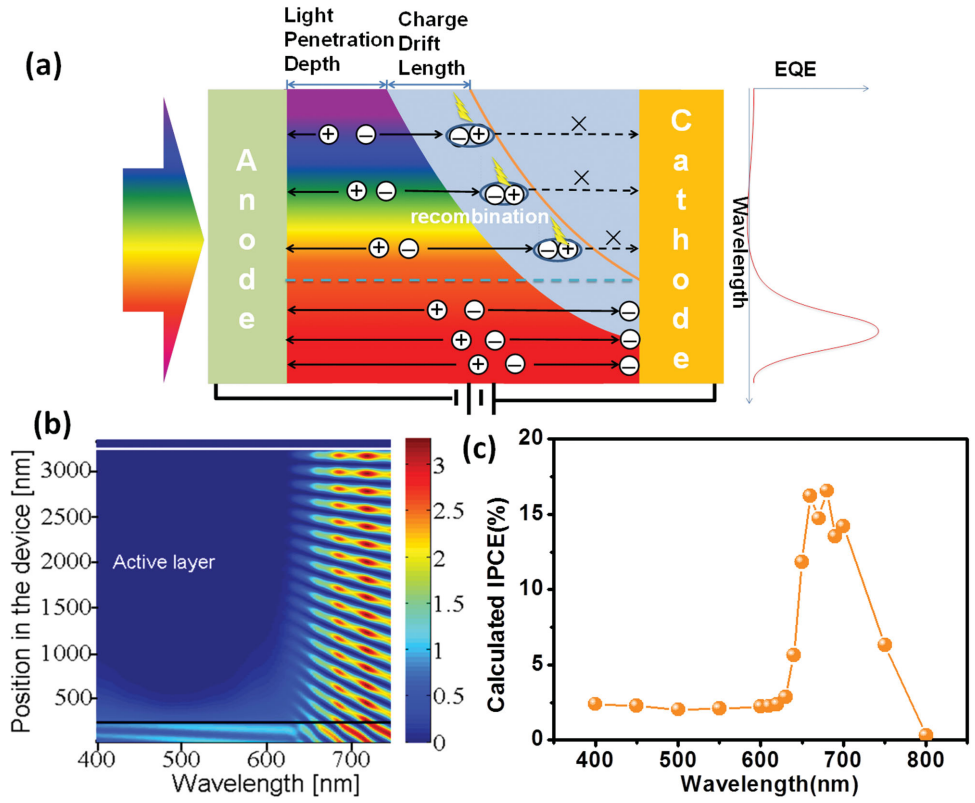

Figure 1. a) Illustration of the narrowband photodetector working principle. b) Distribution of normalized modulus square of optical electric field ($|E(x)^2|$) of active layer interior. c) The calculated IPCE of the photodetector with 3.5 μm thick P3HT:PCBM.

photodetectors, we introduced cadmium telluride (CdTe) quantum dots (QDs) into the P3HT:PCBM bulk-heterojunction films (Figure 2a) to form nanocomposite active layers[9–11]. As illustrated by the energy diagram shown in Figure 2c,d, P3HT acts as electron donor, and both PCBM and CdTe QDs work as electron acceptors. The introduction of CdTe QDs, which have a long electron trapping time, significantly slowed down the recombination of transit holes in P3HT. A photoconductive gain is thus realized because the photoconductive gain is determined by the ratio of the electron–hole recombination lifetime and the hole transit time. These devices also uniquely combine the high gain of a photoconductor and the low noise of a photodiode because of the formation of vertical phase separation in the nanocomposite layer. The enrichment of CdTe at the top surface of the nanocomposite film is shown by the cross-sectional scanning electron micrograph (SEM), which is verified by the energy-dispersive X-ray spectroscopy (EDX) scanning of Cd and Te at a linear scanning mode as shown in Figure 2b. It was clearly observed that the CdTe QDs predominately located at the top surface, which is to be connected to Al cathode. As shown in Figure 2d, photogenerated electrons transfer from P3HT to PCBM and CdTe QDs under illumination. The electrons, including those transferred from P3HT and generated in CdTe QDs, are trapped by CdTe QDs, which cause in situ n-doping of the P3HT:PCBM:CdTe layer at the top surface by forming the space-charge layer. The trapped electrons in CdTe QDs, which are rich close to the cathode, shift the lowest unoccupied molecular orbital (LUMO) of the P3HT downward and align the Fermi energy of active layer with that of the electrode. It causes more holes to be injected into the nanocomposite layer from cathode under a very small applied reverse bias due to the decreased charge injection barrier thickness. This provides a mechanism to form the Ohmic contact, which is a prerequisite for the photoconductor and thus the photoconductive gain.[12] As a result, the photodetector is transformed from a low-noise photodiode in the dark to a high-gain photoconductor under illumination because the Schottky contact was replaced by the Ohmic contact. Since the valance band top of CdTe is deeper than the highest occupied molecular orbital of P3HT, accumulation of CdTe QDs at the interface of nanocomposite/Al will not enhance the dark current due to the blocked hole injection.

Figure 2e shows the absorption spectra of 150 nm thick CdTe, 150 nm thick P3HT:PCBM, and 3.5 μm thick P3HT:PCBM and P3HT:PCBM:CdTe, measured in a transmission mode. Light with wavelength below 630 nm was completely absorbed by the 3.5 μm thick films. There is still relatively weak light absorption in the wavelength range of 630–850 nm, which is either from band tail absorption from P3HT:PCBM, or from CdTe QDs, or due to light scattering. The absorption cutoff of CdTe QDs is 720 nm, which agrees with its diameter of 5 nm. The absorption spectrum of P3HT:PCBM:CdTe thick films is almost the same with that of the P3HT:PCBM thick film other than the small absorption shoulder from CdTe. The absorption spectra provide direct evidence that only red light can penetrate through the whole active layer, while shorter wavelength blue-green light is completely absorbed.

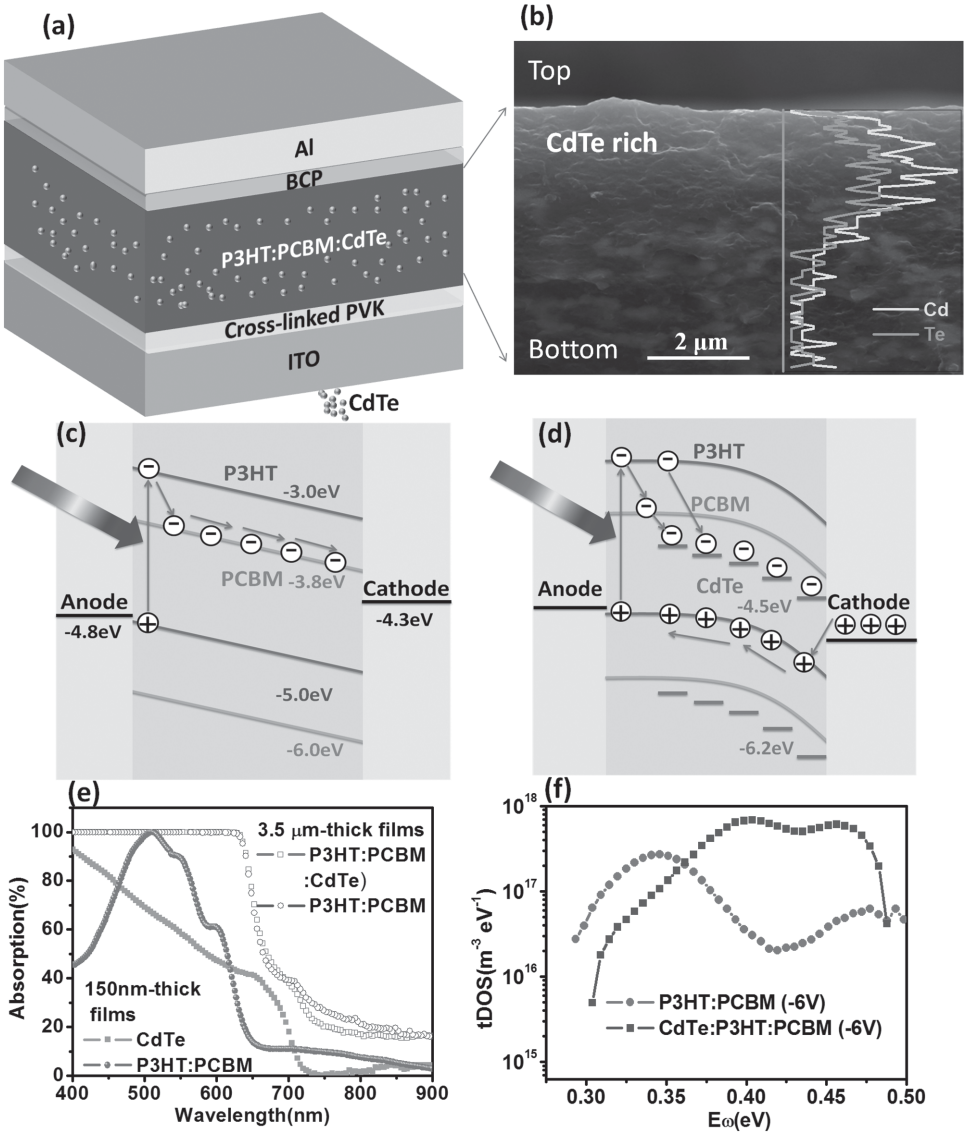

Figure 2. a) Device structure of photodetector. b) Cross-sectional SEM of the blend active layers (CdTe QDs rich in top to Al electrode) combined with EDX with linear scanning mode of Cd and Te. The energy diagram of photodetector under illumination. c) Without CdTe QDs and d) with CdTe QDs. e) Absorption spectra of the CdTe QDs (150 nm), P3HT:PCBM (150 nm), CdTe QDs:P3HT:PCBM (3.5 μm), and P3HT:PCBM (3.5 μm). f) The trap density of state curve versus demarcation energy curve.

In order to identify whether the charge traps were introduced into the devices, the thermal admittance spectroscopy measurement of the photodetectors with and without CdTe QDs was performed. The distribution of the trap states was presented by the calculated trap density of states versus demarcation energy,[13] which is shown in Figure 2f. By comparing the two trap density curves of the devices with or without CdTe QDs, it is observed that a deeper charge trap band from 0.36 to 0.46 eV below band edge was introduced into the device, which should come from the traps in CdTe QDs.[14] Our recent study of CdTe QDs synthesized by the same process verified that the traps are dominated electron traps caused by the quantum confinement of the organic ligand and uncoordinated Cd^{2+} ions on the surface of the QDs.[14]

EQE spectra were measured at different reverse biases to characterize the wavelength-dependent gain of the photodetectors, and the results are shown in **Figure 3**a,b. The P3HT:PCBM devices without CdTe QDs have a narrowband response between 650 and 800 nm, which agrees well with our calculated EQE spectrum. At a reverse bias of –6 V, the peak EQE at 660 nm is about 10%, which is slightly lower than calculated results, because the simulation assumes that all the charges generated within L_d from the Al cathode can be 100% collected. No gain appears in this photodetector and the corresponding peak responsivity of 0.053 A W^{-1} at 660 nm is very small. However, the EQE peak value of the devices with CdTe QDs was dramatically enhanced by 20-folds to around 200% at the same reverse bias. The performance improvement should be

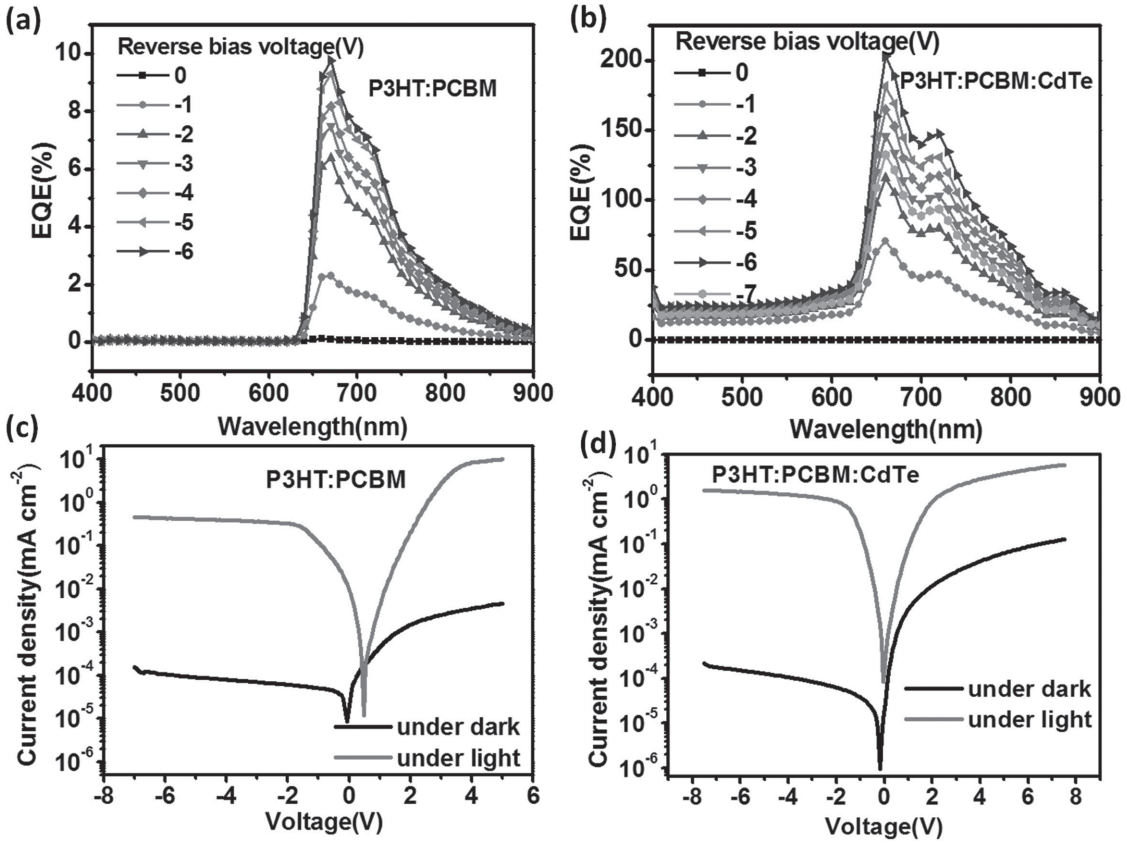

Figure 3. EQEs of photodetectors a) without CdTe QDs and b) with CdTe QDs under reverse bias with a voltage step of 1 V. Photocurrent density at 100 mW cm^{-2} and dark current density of photodetectors c) without CdTe QDs and d) with CdTe QDs.

caused by the trap-induced secondary hole injection. The dark currents in Figure 3c,d show that both the P3HT:PCBM and P3HT:PCBM:CdTe devices have good rectifying characteristic, as well as a low dark current of ≈10^{-7} A cm^{-2} at −6 V, indicating a typical photodiode behaviors. When the P3HT:PCBM device was illuminated under a light intensity of 100 mW cm^{-2} (AM 1.5 G), the photocurrent increased by three orders of magnitude for both reverse bias and forward bias conditions, while the rectification ratio was still in excess of 20 at ±6 V. The P3HT:PCBM device had an open-circuit voltage of 0.6 V, which indicates that the P3HT:PCBM thick-film photodetector still worked in the photovoltaic mode. In striking contrast, the rectification ratio of the P3HT:PCBM:CdTe device decreased significantly to 3 at ±6 V under illumination, and the photovoltage disappeared, which is a direct evidence that the photodetectors transformed from a photodiode to a photoconductor.

To accurately obtain the noise current of photodetectors with the lowest dark current, a fast Fourier transform (FFT) signal analyzer and a current preamplifier were used to record the noise current at different frequencies under −6 V bias. As shown in the inset of **Figure 4**a, the noise currents of the photodetectors with or without CdTe QDs are almost the same (≈3.5×10^{-13} A Hz$^{-1/2}$ at 35 Hz) and are barely sensitive to the frequency. Based on the directly measured noise current and EQE, the specific detectivity (D^*) can be calculated according to the following equations[15]

$$D^* = \frac{\sqrt{AB}}{NEP} \tag{1}$$

$$NEP = \frac{i_n}{R} \tag{2}$$

$$R = \frac{EQE}{\frac{hc}{\lambda q}} \tag{3}$$

where A is the active layer area, i_n is the measured noise current, R is the responsivity, h is the Planck constant, c is the light speed, and λ is the light wavelength. As shown in Figure 4a, D^* at 35 Hz for the photodetectors with CdTe QDs is 7.3×10^{11} cm Hz$^{1/2}$ W^{-1} at 660 nm, which is 20 times higher than that of the devices without CdTe (3.7×10^{10} cm Hz$^{1/2}$ W^{-1}). The NEP of photodetectors is calculated to be 3.3×10^{-13} W Hz$^{-1/2}$, which means the photodetectors should be able to detect the red light intensity of 4.7 pW cm^{-2} because the active layer area of our devices in this study is 7 mm^2.

To further verify whether the photodetectors can actually detect light intensity as low as NEP and the responsivity keeps constant under weak light, we directly measured the signal current under various light intensities with the FFT signal analyzer in the same

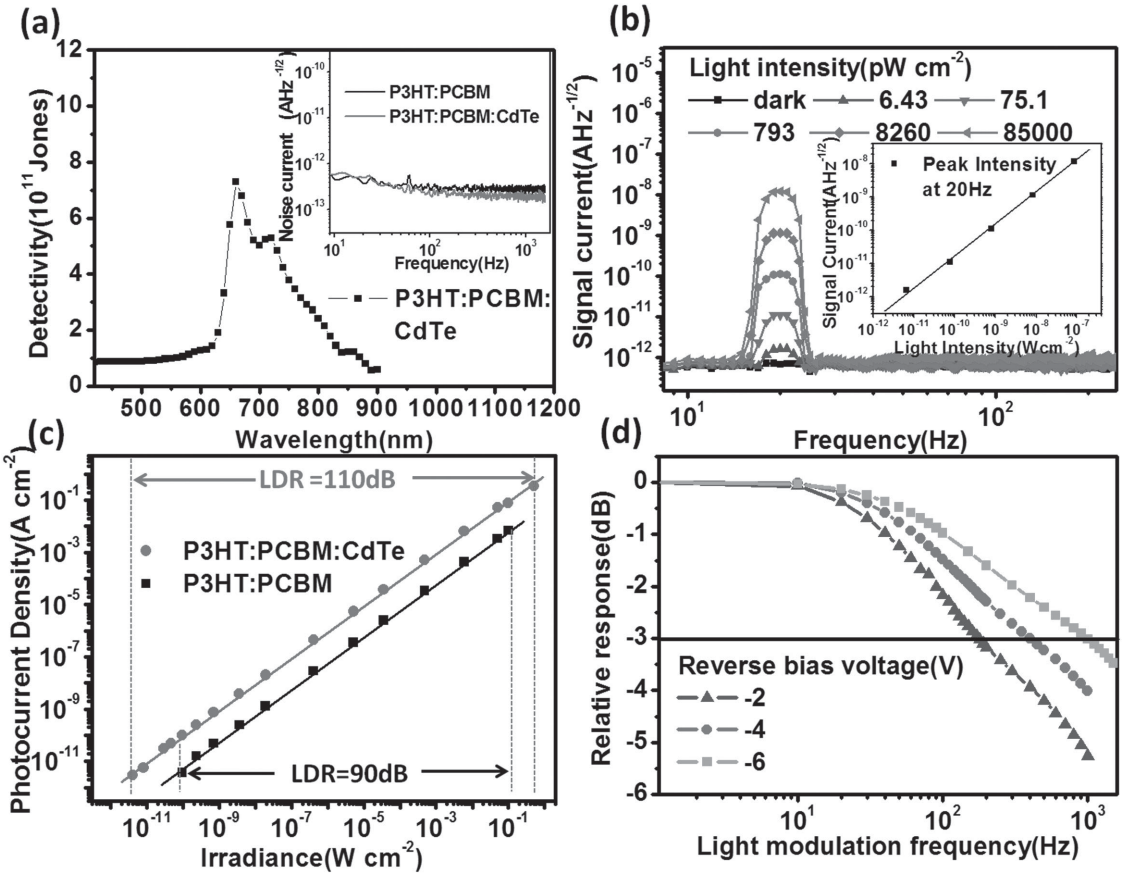

Figure 4. a) The specific detectivity of photodetectors with CdTe QDs under −6 V bias. Inset: the noise current of photodetectors with or without CdTe QDs under −6 V bias. b) The signal current spectra of photodetectors with CdTe QDs under a 660 nm LED at 20 Hz with various light intensities of direct NEP measurement. Inset: the peak signal intensity at 20 Hz obtained from (b) as a function of light intensities. c) The dynamic response of photodetectors with or without CdTe under −6 V bias under a LED illumination of various light intensities. The solid line is linear fitting to the data. d) Normalized response loss of photodetectors with CdTe QDs versus light modulation frequency at a 660 nm LED under (−2, −4, −6 V) bias. The −3 dB point is specified with the solid line.

way as we measured the noise current. The incident light from a red light-emitting diode (LED, electroluminescence peak at 660 nm) was modulated to at 20 Hz by a function generator power source, and the light intensity was tuned by the optical neutral density filters. As shown in Figure 4b, a signal peak appeared at 20 Hz, and it reduced along with the decreasing irradiance. The signal peak merged into the background noise current when the light intensity was reduced to 6.43 pW cm^{-2}. According to the definition of NEP, it represents the lowest light intensity at which the signal of a photodetector can no longer be differentiated from the noise. Thus, the NEP derived here is almost same with the calculated NEP from D^*. Moreover, the light-intensity-dependent signal–intensity plot at 20 Hz was inserted in Figure 4b, which reveals that the signal peak intensities change linearly with the irradiance. To the best of our knowledge, this is first time that NEP was directly measured and agreed well with calculated NEP in polymer–inorganic QDs nanocomposite photodetectors.

We measured the liner dynamic range (LDR) of devices with or without CdTe QDs by recording the steady-state photocurrent under a much large variation of red light intensity at a modulation frequency of 35 Hz. Figure 4c shows that the photocurrent increased linearly with increasing the light intensity from about 5 pW cm^{-2} all the way up to 0.5 W cm^{-2} for the device with CdTe QDs. The 11 orders magnitude linear response corresponds to a large LDR of 110 dB.[16] The LDR of photodetectors without CdTe QDs was also measured and is also shown in Figure 4c. The P3HT:PCBM device had an LDR of 90 dB with linear response from 10^{-10} to 0.1 W cm^{-2}. It is evident that the increased LDR for the device with CdTe QD was caused by the higher responsivity (or EQE) because the noise levels of both types of photodetectors were the same. Finally, the response time of the photodetectors, which is directly related to its frequency response, was measured by the f_{3dB} method, and the result is shown in Figure 4d. The devices were illuminated by the same red LED with varied switching frequency, and the photocurrent of the photodetectors was recorded by a lock-in amplifier. The device response speed is bias dependent because of the changed carrier transit time. The −3 dB cutoff frequency under three reverse bias voltages is 180, 400, and 900 Hz at −2, −4, and −6 V, respectively.[15]

In summary, we reported sensitivity increase of the narrowband red light nanocomposite photodetector by 20 times by

introducing a photoconductive gain. The devices with a gain have improved NEP to 5 pW cm^{-2} at 660 nm and 35 Hz and increased LDR to 110 dB. We believe that this highly sensitive red light photodetector can find niche application in chemical and biological detection.

Supporting Information

Supporting Information is available from the Wiley Online Library or from the author.

Acknowledgements

This work was supported by Defense Threat Reduction Agency under Award No. HDTRA1-14-1-0030 and Office of Naval Research under Award No. N000141210556.

Received: August 3, 2015
Revised: November 13, 2015
Published online: January 18, 2016

[1] L. Zhou, R. Wang, C. Yao, X. Li, C. Wang, X. Zhang, C. Xu, A. Zeng, D. Zhao, F. Zhang, *Nat. Commun.* **2015**, *6*, 6938.
[2] S. O. Kelley, C. A. Mirkin, D. R. Walt, R. F. Ismagilov, M. Toner, E. H. Sargent, *Nat. Nanotechnol.* **2014**, *9*, 969.
[3] P. Alivisatos, *Nat. Biotechnol.* **2004**, *22*, 47.
[4] A. Matsumoto, A. Tamura, R. Koda, K. Fukami, Y. H. Ogata, N. Nishi, B. Thornton, T. Sakka, *Anal. Chem.* **2015**, *87*, 1655.
[5] A. Armin, R. D. J. Vuuren, N. Kopidakis, P. L. Burn, P. Meredith, *Nat. Commun.* **2015**, *6*, 6343.
[6] K. Baeg, M. Binda, D. Natali, M. Caironi, Y. Y. Noh, *Adv. Mater.* **2013**, *25*, 4267.
[7] X. Gong, M. Tong, Y. Xia, W. Cai, J. S. Moon, Y. Cao, G. Yu, C. L. Shieh, B. Nilsson, A. J. Heeger, *Science* **2009**, *325*, 1665.
[8] IUPAC, *Compendium of Chemical Terminology*, 2nd ed., The Gold Book, Wiley, New York **1997**. Online corrected version: (2006) "Beer–Lambert law."
[9] M. He, F. Qiu, Z. Lin, *J. Phys. Chem. Lett.* **2013**, *4*, 1788.
[10] M. He, J. Ge, Z. Lin, X. Feng, X. Wang, H. Lu, Y. Yang, F. Qiu, *Energy Environ. Sci.* **2012**, *5*, 8351.
[11] M. He, F. Qiu, Z. Lin, *Energy Environ. Sci.* **2013**, *6*, 1352.
[12] a) F. Guo, B. Yang, Y. Yuan, Z. Xiao, Q. Dong, Y. Bi, J. Huang, *Nat. Nanotech.* **2012**, *7*, 798; b) R. Dong, C. Bi, Q. Dong, F. Guo, Y. Yuan, Y. Fang, Z. Xiao, J. Huang, *Adv. Opt. Mater.* **2014**, *2*, 549; c) Y. Fang, F. Guo, Z. Xiao, J. Huang, *Adv. Opt. Mater.* **2014**, *2*, 348; d) L. Shen, Y. Fang, Q. Dong, Z. Xiao, J. Huang, *Appl. Phys. Lett.* **2015**, *106*, 023301.
[13] J. A. Carr, S. Chaudhary, *Energy Environ. Sci.* **2013**, *6*, 3414.
[14] H. Wei, Y. Fang, Y. Yuan, L. Shen, J. Huang, *Adv. Mater.* **2015**, *27*, 4975.
[15] *Photonic Devices* (Ed: J.-M. Liu), Cambridge University Press, Cambridge **2005**.
[16] Y. Fang, J. Huang, *Adv. Mater.* **2015**, *27*, 2804.